

Raport stiintific

privind implementarea proiectului in perioada ianuarie – decembrie 2012

PN-II-ID-PCE-2011-3-0735 « Nano-senzori multiparametrici de oxizi metalici obtinuti printehnologii avansate »

Am reusit extinderea sensibilitatii TiO_2 fata de domeniul vizibil al spectrului in vederea detectarii si anihilarii unor reziduri oxidice periculoase care contin ionul Cr (VI). In acest scop am obtinut prin depunere laser pulsata (PLD) filme subtiri de TiO_2 dopate cu ZrO_2 . Dopajul a fost realizat pentru a creste suprafata specifica, aciditatea suprafetei si pentru a modifica proprietatile fotoelectrochimice care conduc la imbunatatirea activitatii fotocatalitice. S-a asigurat totodata o inalta rezistenta la medii agresive, imbunatatirea proprietatilor de absorbtie, stabilitatea la radiatii cu energie mare si proprietati anticorozive.

Pentru realizarea tintelor PLD, am folosit 50% ZrO_2 – 50% TiO_2 wt. Tintele au fost ablate cu un laser KrF* ($\lambda = 248$ nm, $\tau_{FWHM} = 25$ ns, $\nu = 10$ Hz). Ca substraturi am folosit sticla de microscop, curatata succesiv intr-o baie cu ultrasunete in acetona, etanol si apa deionizata timp de 15 min. Substraturile au fost incalzite pana la $600^\circ C$ în timpul depunerii și plasate la 5 cm fata de tinta. Aria depunerii a fost de 10×10 mm². Depunerile au fost efectuate in flux de N_2 , O_2 ori CH_4 de inalta puritate sau amestecuri de 5:1 N_2/CH_4 , 10:1 N_2/CH_4 sau 1:1 N_2/O_2 . Presiunea ambienta a fost stabilizata la o valoare constanta in intervalul 3-10 Pa. Datele despre natura gazului si presiunea mediului ambient in timpul depunerii, impreuna cu valorile benzii interzise, E_g , pentru toate probele preparate se dau in Tabelul I. S-au pregatit serii de cate cinci probe identice pentru fiecare conditie de depunere.

Tabelul I. Codul probei, natura si presiunea gazului, banda interzisa si grosimea filmelor depuse

Cod Proba	Tinta	Natura gazului	Presiunea (Pa)	$E_{g \text{ direct}}$, eV	Grosimea, nm
TZ1	$TiO_2 + ZrO_2$	1:1 N_2/O_2	5	3,45	712
TZ2		O_2	10	3,66	732
TZ3		N_2	10	2,96	702
TZ4		CH_4	10	3,23	648
TZ5		10:1 N_2/CH_4	3	-	676
TZ6		CH_4	5	-	684
TZ7		5:1, N_2/CH_4	10	3,63	692

Filmele au fost caracterizate prin masuratori XRD. Probele TZ3, TZ6, TZ7 si TZ5 au fost caracterizate prin XPS. Activitatea fotocatalitica a filmelor a fost evaluata prin reactia de reducere a ionilor de Cr (VI).

Potrivit observatiilor noastre, absorbtia in domeniul vizibil creste cu continutul de N_2 în amestecurile de gaze (curbele 4, 5 și 6 din Fig. 1). O absorbtie puternica în domeniul VIS a fost observata pentru filmul depus în CH_4 (curba 7 in Fig. 1). Spectrele XRD au confirmat ca toate probele depuse au fost amorfe. Faza

amorfa ar putea fi explicata prin existenta unor particule foarte mici de TiO_2 sau prin prezenta a ZrO_2 in exces care inhiba cristalizarea TiO_2 .

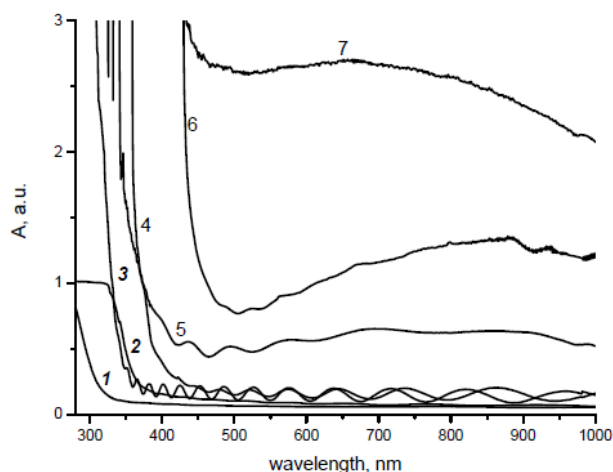


Figura 1. Spectrele de absorbtie pentru filmele de ZrO_2 (1), TiO_2 (2), TZ2 (3), TZ1 (4), TZ7 (5), TZ3 (6), si TZ4 (7)

Din spectrele XPS am observat ca linia Ti 2p a probei depuse in CH_4 pur (Fig. 2b) conține două straturi neechivalente. Contributia dominanta a Ti $2p_{3/2}$ la $E_b = 458,8$ eV (Fig. 2, vârș 3) corespunde speciei Ti^{4+} din TiO_2 . Maximul Ti $2p_{3/2}$ de la 458, 3eV este, de asemenea, atribuit Ti^{4+} (Fig. 2, varș 2), iar scaderea valorii E_b indica cresterea lungimii legaturii Ti-O. Varșul 1 în Fig. 2 ($E_b = 457,5$ eV) apare in spectrele filmelor obtinute in N_2 si amestecurile sale cu CH_4 si poate fi atribuit legaturii O-Ti-N. Prezenta legaturii O-Ti-N corespunde unui inalt grad de performanta fotocatalitic. Spectrele XPS ale probelor obtinute in amestecul de gaze N_2/CH_4 evidenziaza o buna eficienta de incorporare a N_2 în structura, ca urmare a deficitului de oxigen. Cu toate acestea, nu a fost detectata prezenta carbonului atomic in structurile $\text{TiO}_2/\text{ZrO}_2$.

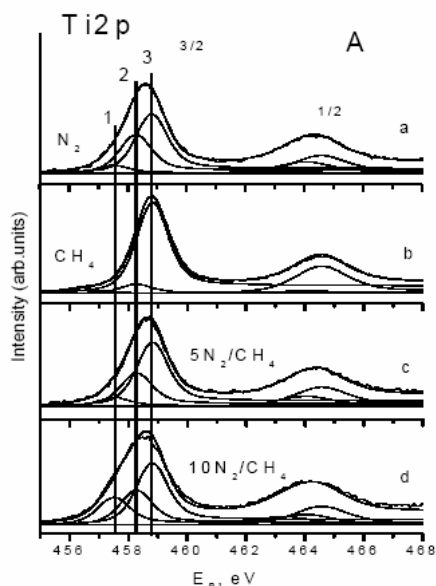


Figura 2. Spectrele XPS ale Ti 2p si energia probelor TZ3 (a), TZ6 (b), TZ7 (c), TZ5 (d)

Activitatea fotocatalitica a filmelor dopate a fost monitorizata prin procesul de fotoreducere a ionilor toxici de Cr (VI) la ionii non-toxici de Cr (III), in medii apoase prin expunere la lumina VIS si UV. Filmele au prezentat un caracter inert sub iradierea cu lumina VIS, activitate similara cu cea a probelor martor. Filmul de ZrO_2 poseda o activitate mult mai mica, comparativ cu filmul de TiO_2 în lumina UV. O imbunatatire a performantei fotocatalitice in comparatie cu filmul de TiO_2 , a fost observata la expunerea la lumina UV a filmului de $\text{TiO}_2/\text{ZrO}_2$ care contine agent dublu de dopaj (TZ5). Cea mai mare rata de reactie (Tabelul II) a fost inregistrata pentru structura cu cel mai mare numar de legaturi de O-Ti-N. Acestea ($E_b = 395,8$ eV) imbunatatesc separarea electron-gol, in timp ce atomii interstitiali de N ($E_b = 400$ eV) incorporati in

structura semiconductoare sunt inerti ca si capcanele de electroni/gol în procesul de fotoreducere la iradierea cu lumina UV si VIS.

<i>Proba</i>	<i>K, sec⁻¹</i>
<i>TZ1</i>	$3,1 \cdot 10^{-5}$
<i>TZ2</i>	$3 \cdot 10^{-5}$
<i>TZ3</i>	$3,5 \cdot 10^{-5}$
<i>TZ4</i>	$3,5 \cdot 10^{-5}$
<i>TZ5</i>	$8,4 \cdot 10^{-5}$
<i>TZ6</i>	$2,2 \cdot 10^{-5}$
<i>TZ7</i>	$2,5 \cdot 10^{-5}$
<i>TiO₂</i>	$7,0 \cdot 10^{-5}$
<i>ZrO₂</i>	$2,2 \cdot 10^{-5}$

Tabelul II. Rata reactiei de fotoreducere a probelor

Putem concluziona ca prezenta unui continut scazut de CH₄ in timpul depunerii (10:1 N₂/CH₄) induce formarea de fragmente O-Ti-N in matricea metalului oxidat, dupa cum reiese din aspectul curbei Ti 2p_{3/2} (E_b = 457,5 eV). De asemenea, incorporarea azotului a indus capcane pentru sarcinile fotogenerate de lumina care au condus la o imbunatatire a detectiei si reducerii fotocatalitice de ioni toxici de Cr (VI) la Cr (III), la iluminarea UV.

Pentru detectarea urmelor de materiale aflate in concentratii foarte mici, am dezvoltat cu prioritate pe plan international o noua metoda imagistica bazata pe folosirea intensitatilor diferite ale luminii evanescente dintr-un ghid optic (lb. eng. Differential Evanescent Light Intensity, DELI). Aceasta metoda este o tehnica de microscopie optica bazata pe capturarea campului optic extras din straturile de nanomateriale prezente pe un ghid de unda din campurile evanescente. Materialele pot fi in stare solida, dar si gazoasa sau lichida si de aceea metoda are mare potential in dezvoltarea de noi tipuri de senzori prin folosirea unei tehnologii simple si ieftine. Prezentam in continuare principiile DELI si aplicarea ei la detectarea unor mici cantitati de nanoparticule de aur amorf, selenium amorf si polietilena, materiale de mare interes pentru dezvoltarea de senzori performanti atat electrici cat si optici. DELI utilizeaza fenomenul de reflexie totala interna prin care se produc unde evanescente. Prin DELI se pot inregistra caracteristicile intensitatii optice a luminii dispersate de particulele depuse pe un substrat de la un fascicul luminos care se propaga printr-un substrat de sticla ce joaca rolul de ghid de unda.

In experimente au fost comparate profile DELI ale unor nanostructuri apartinand unor clase diferite de materiale - conductoare, semiconductoare si izolatoare: Au amorf (a-Au), Se amorf (a-Se) si polietilena (PE), obtinandu-se parametrii caracteristici ai campului evanescent cu ajutorul unui model fenomenologic.

Fasciculul de lumina, din spectrul vizibil, introdus in ghidul de unda a provenit de la o lampa cu quart-halogen GE-Thorn, model DDL, cu un iluminator de fibra, model Volpi AG, cu o intensitate I₀ = 3.75 W/cm²

in domeniul spectral (400-800) nm, in varful fibrei. Imaginea optica a luminii evanescente provenind de la ghidul de unda a fost capturata de un microscop Leica Wild M3Z, cu o marire de 65-400X, echipat cu o camera CCD, cu raspuns calibrat la lungimea de unda de 555 nm.

Filmele a-Au au fost obtinute prin pulverizare cu magnetron, cele a-Se, prin fotodepunere iar straturile de PE prin evaporarea laser pulsata asistata de o matrice.

In Fig. 3 sunt prezentate imagini DELI ale unor nanostructuri a-Au, insotite de profile 1D. Densitatea optica integrata si normalizata (lb. eng. Normalized Integrated Optical Density, NIOD) s-a obtinut prin integrarea intregii suprafete si normalizarea intr-un profil efectiv pe nivele de gri ale zonei investigate:

$$NIOD = \frac{\int D(x,y) dx dy}{S} \quad (1)$$

unde $D(x,y)$ este densitatea optica iar S , suprafata zonelor 2D.

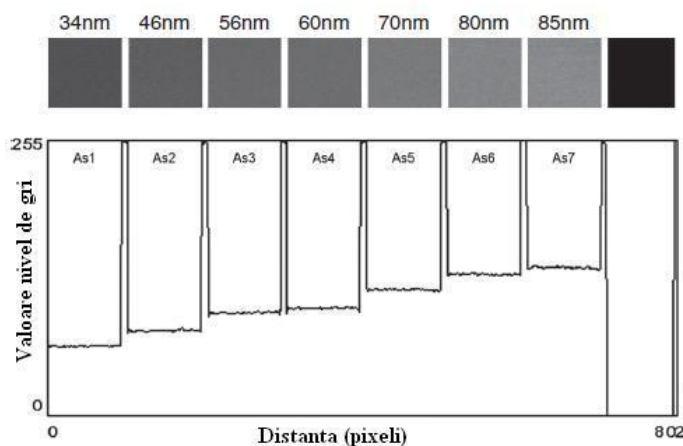


Figura 3. Imagini DELI 2D ale profilelor suprafetelor filmelor a-Au pentru grosimi in domeniul (34–85) nm si profile 1D mediate pe coordonata y corespunzatoare fiecarei imagini 2D. Zona intunecata a fost folosita in scopul calibrarii

In tehnica DELI, puterea luminii extrase din ghidul de unda depinde de grosimea si numarul de nanoparticule prezente pe suprafata. Modelul fenomenologic presupune ca vectorul evanescent situat in aerul din vecinatatea ghidului de unda este perturbat de particulele depuse iar intensitatea luminii evanescente extrase $I_z(x,y)_{det}$ care ajunge la detectorul CCD este data de:

$$I_z(x,y)_{det} = I_0 \eta(x,y) \quad (2)$$

unde I_0 este intensitatea campului optic de la interfata ghid de unda/material; iar $\eta(x,y)$, eficienta de extractie a fotonilor in functie de materialul depus.

In general, pentru grosimi < 200 nm, se poate neglija absorbtia optica in filme:

$$\eta(x,y) = \frac{h(x,y)}{h_0} \gamma \quad (3)$$

unde $h(x,y)$ este grosimea materialului in directia z in punctul (x,y) pe suprafata ghidului de unda; iar constanta γ , abilitatea nanomaterialului de a extrage fotonii evanescenti din ghidul de unda.

In cazul in care absorbtia optica se poate neglija, ceea ce este valabil pentru majoritatea straturilor nanometrice groase, raportul NIOD pentru doua grosimi h_1 si h_2 este:

Valorile obtinute pentru parametrul γ si adancimea de penetrare efectiva a fotonului evanescent, d , sunt sumarizate in Tabelul III.

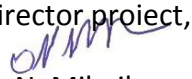
Tabelul III. Valorile parametrilor γ si d pentru diferite tipuri de materiale si grosimi

Material	a-Au	a-Se	PE
η_1	38.90	30	32.7
h_1 , nm	26.3	40	83
η_2	73.47	80	68.3
γ , nm ⁻¹	0.0284	0.0116	0.00779
d , nm	35.2	86.5	128.3

Dupa cum se poate observa, valoarea d pentru a-Au este mai mica decat pentru a-Se si PE, ceea ce inseamna ca metalul are un domeniu de extractie evanescenta mai scurt in raport cu celelalte doua materiale. Putem concluziona ca, pentru evaluarea cu ajutorul tehnicii DELI a grosimilor nanometrice pentru diferite clase de materiale, ne putem ghida dupa valoarea caracteristica a parametrului $d \approx \gamma^{-1}$.

Pentru straturile izolatoare, tehnica prezinta un domeniu mai larg de interactiune cu fotonii evanescenti in comparatie cu semiconductorii si conductorii. Astfel, prin metoda DELI se poate masura profilul filmelor cu grosimi de pana la 200 nm. Nu exista niciun risc de degradare a filmelor deoarece prin DELI acestea nu sunt expuse direct actiunii intense a luminii sau fasciculelor de electroni. Aceasta tehnica este mult mai usoara si mai economica pentru determinarea profilelor filmelor nanometrice in comparatie cu SEM si AFM si este potrivita in special pentru profile ale unor suprafete mari utilizate in aplicatii industriale.

1. „*Measuring Nanolayer Profiles of Various Materials by Evanescent Light Technique*”, N. Mirchin, B. Apter, I. Lapsker, V. Fogel, U. Gorodetsky, S. A. Popescu, A. Peled, G. Popescu-Pelin, G. Dorcioman, L. Duta, A. Popescu, I. N. Mihailescu, *Journal of Nanoscience and Nanotechnology*, Vol. 12(3), pp. 2668–2671, 2012;
2. “*Nanoprofiles evaluation of pulsed laser deposited ZnO films using an evanescent light method*”, N. Mirchin, A. Peled, L. Duta, G. Dorcioman, A.C. Popescu, I.N. Mihailescu, trimis spre publicare la *Applied Optics*, November 2012.
3. “*TiO₂/ZrO₂ thin films synthesized by PLD in low pressure N-, C- and/or O-containing gases: structural, optical and photocatalytic properties*”, O. Linnik, I. Petrik, N. Smirnova, V. Kandyba, O. Korduban, A. Eremenko, G. Socol, N. Stefan, C. Ristoscu, I. N. Mihailescu, C. Sutan, V. Malinovski, V. Djokic, Dj. Janakovic, *Digest Journal of Nanomaterials and Biostructures*, Vol. 7(3) (July–September 2012), 1343-1352 (2012)

Director proiect,

 Prof. Dr. Ion N. Mihailescu

TiO₂/ZrO₂ THIN FILMS SYNTHESIZED BY PLD IN LOW PRESSURE N-, C- AND/OR O-CONTAINING GASES: STRUCTURAL, OPTICAL AND PHOTOCATALYTIC PROPERTIES

OKSANA LINNIK^a, IRINA PETRIK^a, NATALIA SMIRNOVA^a,
VIKTOR KANDYBA^b, OLEKSANDR KORDUBAN^b, ANNA EREMENKO^a,
GABRIEL SOCOL^c, NICOLAIE STEFAN^c, CARMEN RISTOSCU^{c*},
ION N. MIHAILESCU^c, CLAUDIU SUTAN^d, VIOREL MALINOVSKI^d,
VELJKO DJOKIC^e, DJORDJE JANAKOVIC^e

^a*O. O. Chuiko Institute of Surface Chemistry, National Academy of Science of Ukraine, 17 General Naumov str., Kyiv, 03164, Ukraine*

^b*G.V. Kurdyumov Institute of Metallophysics, National Academy of Sciences of Ukraine, Acad. Vernadsky blvd. 36, Kyiv, 03680, Ukraine*

^c*National Institute for Lasers, Plasma and Radiation Physics, 409 Atomistilor street, Magurele, PO Box MG-54, RO-77125, Ilfov, Romania;*

^d*University of Pitesti, Research Centre for Advanced Materials, Targul din Vale Street, No 1, 110040, Pitesti, Arges, Romania*

^e*Faculty of Technology and Metallurgy, University of Belgrade, Karnegijeva 4, 11000 Belgrade, Serbia*

Doped TiO₂/ZrO₂ films were obtained by Pulsed Laser Deposition method under different synthesis conditions. The onset of absorption spectra was red shifted for the films obtained in N₂ containing gas mixtures, while a broad absorption in visible was observed in the case of films deposited in CH₄ atmosphere. The presence of O-Ti-N bonds revealed by XPS corresponded to the highest photocatalytic performance. XPS spectra of the samples obtained in N₂/CH₄ gas mixtures evidenced a more effective incorporation of nitrogen in the structure due to oxygen deficiency. Nevertheless, no atomic carbon presence in the TiO₂/ZrO₂ structures has been detected.

(Received June 20, 2012; Accepted September 6, 2012)

Keywords: TiO₂/ZrO₂ thin films, N- and C-doping, photocatalytic activity, toxic Cr(VI) ions reduction

1. Introduction

Heterogeneous photocatalysis based on the interaction of semiconductor particles with light has focused an enormous attention in environmental and energy-storing research fields. Photocatalysis is applied for the destruction and redox transformations of highly toxic inorganic or organic compounds, as well as for hydrogen production and solar energy conversion to electricity [1-4]. We note that titanium dioxide is an inexpensive semiconductor material, non-toxic, resistant to photocorrosion which is possessing high oxidative power. However, TiO₂ absorbs only 4 % of ultraviolet light and it is inert in the whole visible range of the solar spectrum. The challenge was therefore to extend the sensitivity of TiO₂ towards the visible range of the spectrum. One well-known approach is the doping with transition metals (such as chromium, iron, nickel, vanadium...). Nevertheless, these doped materials suffer of thermal instability and carrier recombination centres augmentation [5-12]. On the other hand, we have shown that the nitrogen

*Corresponding author: carmen.ristoscu@inflpr.ro

and carbon doping of TiO₂ thin films synthesized by pulsed laser deposition (PLD) significantly improved the photocatalytic activity under UV-vis irradiation [12]. As known, PLD allows for obtaining high purity thin films of single or multicomponent materials [13-15]. Incorporation of ZrO₂ in TiO₂ lattice was reported to enhance the specific surface area, the surface acidity and modify the photoelectrochemical properties leading to the improvement of the photocatalytic activity [16]. High resistance against aggressive media, regulation of the structure-sorption properties of the composites, stability to high-energy radiation and high anticorrosive properties of the photocatalytic coatings were gained by the mixing TiO₂ with ZrO₂ [17].

We report herewith on the PLD synthesis of TiO₂/ZrO₂ thin films doped with N₂. The photocatalytic activity of the obtained structures was tested for chromium toxic ions reduction.

2. Experimental

2.1. PLD

PLD experiments were carried out in a stainless steel irradiation chamber. Prior to any deposition, the chamber was evacuated down to a residual pressure of 10⁻⁴ Pa.

We used 50% ZrO₂ – 50%TiO₂ wt composite targets. The targets were ablated by a KrF* laser source ($\lambda = 248$ nm, $\tau_{FWHM} = 25$ ns, $\nu = 10$ Hz). The laser beam was directed at 45° on target surface by a 30 cm AR coated MgF₂ lens placed outside the irradiation chamber. The incident laser fluence was set at 1.6 J/cm². Series of 20,000 subsequent laser pulses were applied for the deposition of each film. During the multipulse laser ablation the targets were rotated with a frequency of 0.3 Hz and translated along 2 orthogonal axes to avoid drilling and ensure a uniform deposition, free of particulates.

Previous to introduction inside the deposition enclosure, the microscope glass substrates were successively cleaned in an ultrasonic bath in acetone, ethanol and deionized water for 15 min. The substrates were heated up to 600 °C during deposition and placed at 5 cm from target. The deposition area was 10x10 mm².

The depositions were performed in a low flux of high purity N₂, O₂, CH₄ or mixtures of 5:1 N₂/CH₄, 10:1 N₂/CH₄ or 1:1 N₂/O₂. The gas flux was monitored with MKS 100 controllers and the ambient pressure was stabilized to a constant value within the 3-10 Pa range. The data about the ambient gas nature and pressure during deposition together with the inferred values of the bandgap for all prepared samples were collected in Table I. In order to provide a statistically meaningful data set, we have prepared a series of five identical samples for each deposition condition.

Table I. Samples labeling, deposition gas nature and pressure, band gap energy and thickness of deposited films

Sample Code	Target	Deposition ambience	Pressure (Pa)	E_g direct, eV	Thickness nm
TZ1	TiO ₂ +ZrO ₂	1:1 N ₂ /O ₂	5	3.45	712
TZ2	TiO ₂ +ZrO ₂	O ₂	10	3.66	732
TZ3	TiO ₂ +ZrO ₂	N ₂	10	2.96	702
TZ4	TiO ₂ +ZrO ₂	CH ₄	10	3.23	648
TZ5	TiO ₂ +ZrO ₂	10:1 N ₂ /CH ₄	3	-	676
TZ6	TiO ₂ +ZrO ₂	CH ₄	5	-	684
TZ7	TiO ₂ +ZrO ₂	5:1 N ₂ /CH ₄	10	3.63	692

2.2. UV-Vis spectrophotometry

Optical spectra of the films were measured with a double beam spectrophotometer (Lambda 35, PerkinElmer) in the wavelength range of 190–1200 nm. To evaluate the band gap

energy, the spectral dependences of the absorption coefficient (α) from $\alpha = 4\pi k/\lambda$ were obtained. The square and the square root of the absorption coefficient were plotted vs the light energy in the case of a direct and indirect semiconductor, respectively. In our case, the use of the square root is necessary to obtain the required linear relationship pointing on a direct electronic transition. The absolute error of band gap calculations was estimated as ± 0.02 .

2.3. XRD

The XRD spectra of deposited structures were acquired with a Rigaku Ultima IV diffractometer equipped with multilayer structure (Cross Beam Optics) and with high precision vertical goniometer (θ - θ) of 285 mm radius. For phase analysis, the spectra were acquired in parallel beam setup, $\text{CuK}\alpha$ radiation at grazing incidence ($\alpha = 1^\circ$) using the multi-purpose attachment (MPA) for thin films. Working conditions were set as anodic voltage $U_a = 4$ kV, anodic current $I_a = 30$ mA, $2\theta \in (15^\circ, 85^\circ)$ or lower depending on sample, $\Delta(2\theta) = 0.05^\circ$ and acquisition time per step $\tau = 2$ s.

2.4. XPS

XPS spectra were explored with an electron spectrometer with PHOIBOS-100_SPECS energy analyzer. Nonmonochromatic $\text{MgK}\alpha$ X-rays (1253.6 eV) were employed at $P = 200$ W. All the peaks of XPS spectra were charge corrected using C 1s peak position as the reference point. Surface charge of the tested samples was in the range of 1.5-2.7 eV. Charge neutralization was performed using flood gun FG15/40 SPECS and aluminium screen-trap onto the sample. The vacuum in the working chamber was 2×10^{-7} Pa.

Spectra of Ti2p- and Zr3d- levels were deconvoluted into connected with each other pairs of the components with consideration their spin-orbit splitting and parameters (Ti2p: $\Delta E = 5.76$ eV; $I_{1/2}/I_{3/2} = 0.5$, FWHM = 1.28 eV; Zr3d: $\Delta E = 2.4$ eV; $I_{3/2}/I_{5/2} = 0.66$, FWHM = 1.3 eV) Spectra of O1s- and N1s- levels were deconvoluted on the components with FWHM = 1.4 eV. The XPS signals were fitted using Gaussian-Newton method in the mode of bounded parameters. Variation of component intensity and bond energy was performed. Width of the components and ratio contribution of Gaussian-Lorentzian distribution for certain atoms of the tested samples in the process of spectrum deconvolution were fixed. The component square was determined after background subtraction by Shirley method. [18].

2.5. Photocatalytic activity

Photocatalytic activity of the films was assessed via Cr(VI) ions reduction reaction. The film was immersed in 40 ml of an aqueous solution of potassium bichromate (in all experiments, the initial concentration of bichromate ions was 2×10^{-4} M) and the reducing agent (disodium salt of ethylenediaminetetraacetic acid (Na_2EDTA)) in the molar ratio 1:1 adjusted to $\text{pH} \geq 2$ by perchloric acid. The reaction temperature was kept constant (25°C) during the experimental procedure. The change of Cr(VI) ions concentration was monitored with a Lambda 35 UV-vis spectrophotometer (PerkinElmer) every 20 min. The reaction rate was attributed to pseudo-first order and inferred from the absorption intensity at $\lambda = 350$ nm. The film was immersed in the solution until complete adsorption in the dark occurred, and then irradiated by 1000 W middle- pressure mercury lamp for 120 min. The distance lamp - reactor was set at 90 cm. Two blank experiments were carried out: the catalytic reduction of dichromate ions (dark condition), and photoreduction reaction (a bare glass was used instead of film). No significant changes in the absorption spectra of the liquid were observed for both blanks. For testing the visible light sensitivity, a filter transmitting light with $\lambda > 380$ nm was introduced in the photocatalytic setup.

3. Results and discussion

The film thickness was measured by profilometry and found to be in the range 648 – 732 nm (Table I).

3.1. UV-Vis spectrophotometry

TiO₂/ZrO₂ films prepared in ambient N₂ and/or CH₄ atmospheres exhibited a different extension degree in the visible light absorption spectra. As visible from Fig. 1, the absorption onset at 340 nm for undoped TiO₂/ZrO₂ film deposited in 10 Pa O₂ (curve 3) coincides with that of pure TiO₂ film (curve 2) (synthesized on glass substrate heated at 600 °C from a TiO₂ target in 20 Pa oxygen). The pure ZrO₂ film (curve 1 in Fig. 1) was obtained from a ZrO₂ target in 20 Pa oxygen on glass substrates kept during deposition at 600 °C. A red shift up to 385 and 460 nm was observed for the TiO₂/ZrO₂ films deposited in ambient 1:1 N₂/O₂ (curve 4) and N₂ (curve 6), respectively.

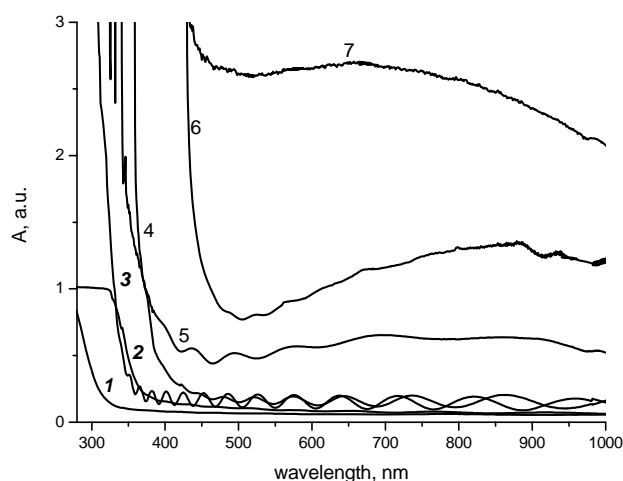


Fig. 1. Absorption spectra of ZrO₂ (1), TiO₂ (2), TZ2 (3), TZ1 (4), TZ7 (5), TZ3 (6), and TZ4 (7) films

According to our observations, the absorption in the visible region increases with the N₂ content in the ambient gas mixtures (compare curves 4, 5 and 6 in Fig. 1). A broad absorption in the visible region was noticed for the film deposited in CH₄ (curve 7, Fig 1). The narrowing of the band gap energy without any shift of the conduction and valence bands position is considered an effect of N - generated mid-gap level [19].

The influence of the doping agent nature and content was observed in the varied band-gap energy values (Table I). These values, E_g , were calculated by extrapolating the linear parts of the $(\alpha h\nu)^2 \sim f(h\nu)$ curves, i.e. assuming the direct electronic transition. On the other hand, for the doped composite samples TZ5 and TZ6, the calculation of E_g was impossible because of the strong absorption in the visible region.

3.2. XRD

All films were amorphous as confirmed by the recorded XRD patterns (Fig. 2). The amorphism could be explained by the existence of very small TiO₂ particles or by the presence of ZrO₂ in excess inhibiting the TiO₂ crystallization [20, 21]. Some incipient crystallization corresponding to the (101) line of ZrO₂ was observed for all samples. We cannot rule out the possible formation of some TiO₂ nanoparticles undetectable by XRD. Indeed, as mentioned in previous section, the onset of the absorption spectra of TiO₂/ZrO₂ and the TiO₂ films coincides

(compare curves 2 and 4 in Fig. 1), while the binding energies of the Ti2p levels in both TiO₂/ZrO₂ and TiO₂ anatase are overlapping [12]. The crystallization of metal oxide was therefore not observed in bulk, but the anatase phase could appear on the surface (1-2 nm in depth).

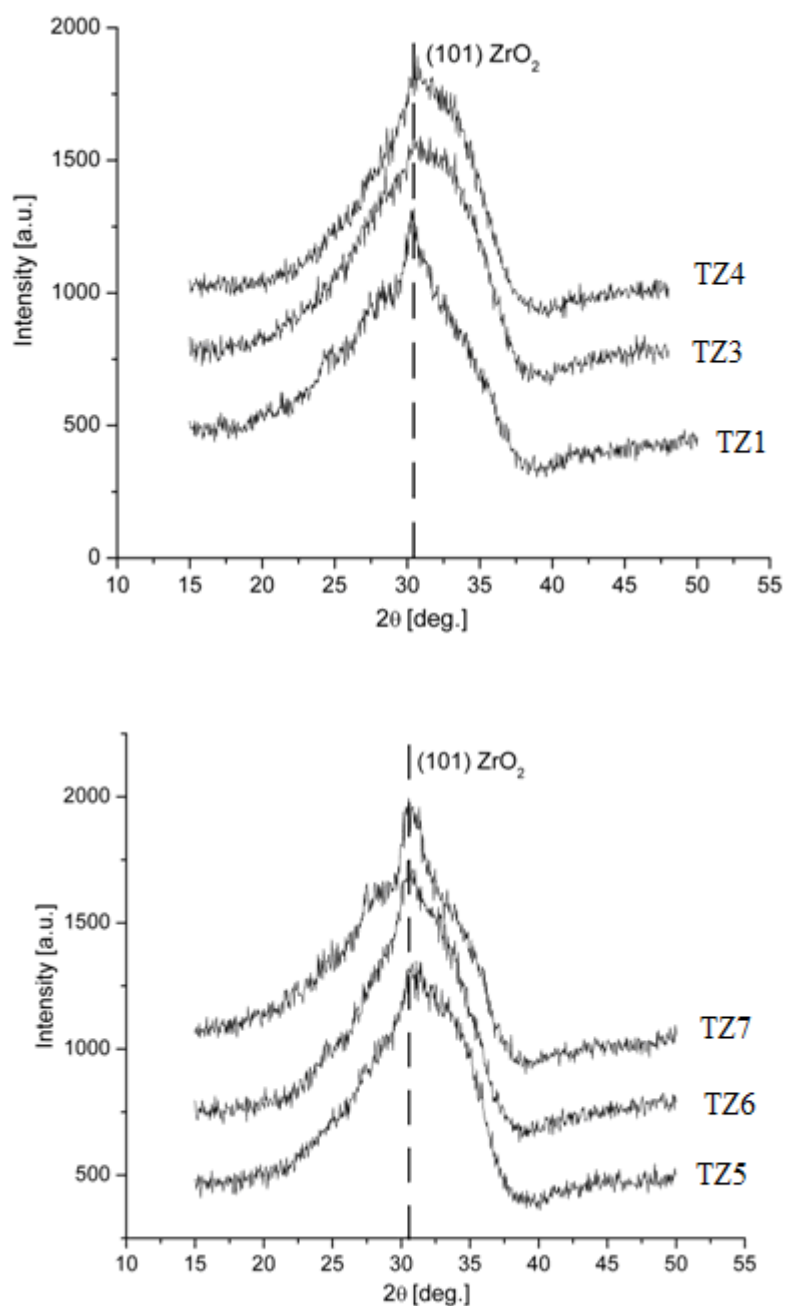


Fig. 2. XRD spectra of deposited TiO₂/ZrO₂ thin films

3.3. XPS

To investigate the surface structure and understand the origin of possible differences in the photocatalytic activity of samples, the films synthesized in pure N_2 (TZ3), CH_4 (TZ6) and their mixtures (TZ7 and TZ5) have been submitted to XPS investigations.

As shown the Ti 2p line of the sample synthesized in pure methane (Fig. 3A, b) contains two nonequivalent states. The dominating contribution in $Ti2p_{3/2}$ XPS spectra assigned to $E_b = 458.8$ eV (Fig. 3A, peak 3) corresponded to Ti^{4+} species in TiO_2 . The Ti $2p_{3/2}$ peak at 458.3 eV is also assigned to Ti^{4+} (Fig. 3A, peak 2), the decrease of E_b value indicates on the increase of Ti-O bond length. These peaks were also characteristic to undoped anatase film obtained in our laboratory by PLD method [12].

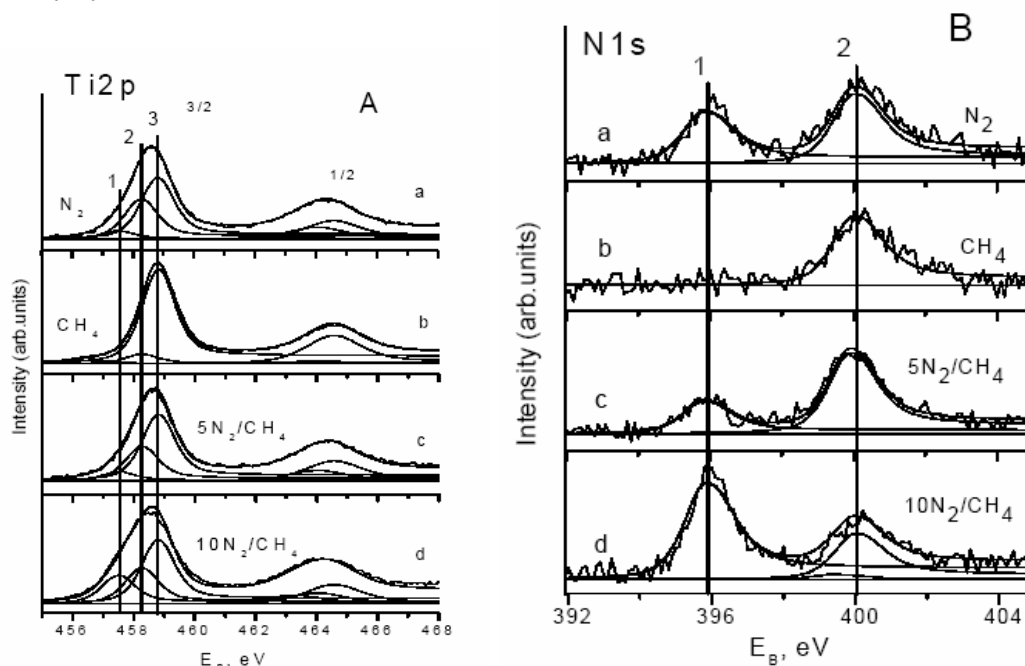


Fig. 3. XPS spectra of $Ti2p$ (A) and $N1s$ (B) energy for the samples TZ3 (a), TZ6 (b), TZ7 (c), TZ5 (d).

The peak 1 in Fig. 3A ($E_b=457.5$ eV) appeared in the spectra of the films obtained in N_2 and its mixtures with CH_4 could be assigned to the O-Ti-N bonds, as mentioned in Refs. 22-24. Appearance of deconvoluted peak at this range of E_b values in Ti 2p line was also sign to the formation of titanium Ti^{3+} species suggesting the existence of oxygen vacancies [25]. In our previous study the Ti2p peak at 457.5 eV was not registered for undoped titania film [12]. In addition to this, N1s spectra of the films synthesized only in N_2 contained gas mixtures indicate the nitrogen atom incorporation in titania. Thus, we suggest that the peak at 457.5 eV belongs to the Ti-N bond rather than oxygen vacancies. It must be emphasized that spectra of the TZ.5 sample contains the most contribution of the peaks such as $Ti2p_{3/2}$ at $E_b= 457.5$ eV and N1s with $E_b = 395.8$ eV (tables II) indicating more nitrogen incorporation in the bonds. The comparison of XPS data of TZ3, TZ5 and TZ7 samples points out to the existence of an optimum content of methane in the process of the N-doped semiconductor films synthesis by PLD method. It is suggested that the carbon from N_2/CH_4 mixture interacts with oxygen from TiO_2 leading to the formation of an oxygen deficient lattice and, in turn, assists an efficient embedding of nitrogen atom. This could result in the higher efficiency of O-Ti-N as compared to O-Ti-O fragments formation.

The binding energy of $Zr3d_{5/2}$ peak for all samples (not shown here) is 182.3 eV corresponding to Zr^{4+} states in ZrO_2 [26]. This correlates with the results reported herein [27] where only the peak with $E_B Zr3d_{5/2}= 182.3$ eV was observed at high content of zirconium in titania matrix. ...

The peak 1 with 395.9 eV is pointing to the Ti-N bond formation by the atomic substitution of oxygen with nitrogen [28, 29] as shown on N1s spectra (Fig. 3B). The peak 2 of nitrogen (400.0 eV) (Fig. 3B) was assigned [29, 30] to the nitrogen adsorption from air in the film. The spectrum of the sample TZ6 deposited in methane also contains interstitial nitrogen resulting from N₂ adsorption in the forming structure. It follows that N-doping does not occur in the gas phase, but rather in the film structure after heating [31]. Almost equal intensity of the peaks at 395.8 and 400.0 eV was observed for the sample TZ3 deposited in pure N₂. More Ti-N bonds were noticed in case of sample TZ5 as the intensity of the peak at 395.9 eV was raising (Table II). As in the case of Ti 2p spectra, this indicates that carbon species forming as a result of laser action react with oxygen one causing the subsequent oxygen substitution by nitrogen atoms. This mechanism is supported by the XPS evidence according to which the intensity of peak at 395.9 eV was lower in case of samples TZ3 vs. TZ5, even though the synthesis was conducted in the first case in a pure N₂ atmosphere

Table II. XPS relative intensities of Ti2p_{3/2} - N1s- and O1s- peaks

E _b /Sample	TZ3	TZ5	TZ6	TZ7
	I, (%)	I, (%)	I, (%)	I, (%)
Ti2p _{3/2} 457.5 eV	7.5	23.5	-	8.1
Ti2p _{3/2} 458.3 eV	36.9	27.8	9.0	31.7
Ti2p _{3/2} 458.8 eV	55.6	48.7	91.0	60.2
N 1s 395.8 eV	42.5	67.6	-	28.7
N 1s 400.0 eV	57.5	32.4	100	71.3
O 1s 530.1 eV	66.5	67.4	89.9	58.9
O 1s 531.7 eV	17.4	12.9	-	17.7
O 1s 532.5 eV	11.0	15.5	10.1	15.0
O 1s 533.2 eV	5.1	4.2	-	8.4

The peak of O1s spectra with E_b=530.1 eV (Table II) is assigned to O²⁻ species of titanium-oxygen and zirconium-oxygen bonds. The binding energy at 531.7 eV is attributed to the lower electron density oxygen species as "O" compensating for deficiencies at the TiO₂ surface [26] or the presence of OH groups. The peaks at E_b=532.5 eV and E_b=533.2 eV are connected with OH-groups and H₂O, respectively. The lowest content of O⁻, OH⁻ species and H₂O for sample TZ6 is indicative for a less defective surface in comparison with the other films.

Miyauchi *et al.* [32] synthesized carbon-doped titania by oxidizing TiC and observed the C1s peak at a much lower binding energy (281.8 eV). They assigned this peak to the Ti-C bond in carbon-doped anatase phase. The other two features at 288.1 and 286.3 eV were attributed to C-N and C-O bonds, respectively. In our case, the elementary carbon peaking at 285 eV [33] and a small fraction of oxidized carbon (286.4 eV) [30] were observed (not shown here) by scanning the C1s region. We assumed that no Ti-C bonds were present in the structure of the films. It must be emphasized that the C1s signal was not detected for the film obtained in pure nitrogen (TZ3).

Overall, the presence of nitrogen as well as its mixture with methane in the synthesis chamber leads to the appearance of Ti2p_{3/2} state with E_b=457.5 eV and N 1s state with E_b=395.8 eV, (table II) reflecting the formation of O-Ti-N bonds in the oxide matrix. The TZ5 film synthesized at minimum methane content in N₂/CH₄ mixture and minimum pressure exhibits the maximum reaction rate constant of photodegradation as well as the highest possible distribution of Ti2p and N1s states connected to O-Ti-N bonds. Interaction of formed under laser pulse carbon atoms and radicals with oxygen atoms of O-Ti-O fragments leads to the formation of oxygen vacancies and increase of O-Ti-N fragments is suggested. Stronger Zr-O bond is invariably remained at this condition.

3.4. Photocatalytic activity

The photocatalytic activity of doped films was monitored in the process of the toxic Cr(VI) ions photoreduction to non-toxic Cr(III) ions in aqueous media by exposure to visible or UV light. The films were inert under visible light irradiation showing an activity similar to that of blank sample. Bare zirconium oxide film possessed much lower activity comparing to bare TiO₂ film under UV light. An improvement of the photocatalytic performance compared to TiO₂ film was observed under UV light exposure of TiO₂/ZrO₂ film containing double doping agent (TZ5). The highest reaction rate constant (Table III) was reached for the structure with the largest number of O-Ti-N bonds. We suggest that the O-Ti-N bonds ($E_b = 395.8$ eV) improve the electron-hole separation, while the interstitial N atoms ($E_b = 400.0$ eV) incorporated in semiconductor structure are inert as the electron/hole traps in photoreduction under UV and Vis - light irradiation.

Table III. The reaction rate constant of studied samples for Cr⁶⁺ to Cr³⁺ photoreduction under full light irradiation

Sample	K, sec ⁻¹
TZ1	3.1*10 ⁻⁵
TZ2	3.0*10 ⁻⁵
TZ3	3,5*10 ⁻⁵
TZ4	3,5*10 ⁻⁵
TZ5	8,4*10⁻⁵
TZ6	2,2*10 ⁻⁵
TZ7	2,5*10 ⁻⁵
TiO ₂	7,0*10 ⁻⁵
ZrO ₂	2,2*10 ⁻⁵

Thus, the TiO₂ band-gap narrowing is mandatory for extending the photocatalytic action to visible light. Nevertheless, other factors such as an effective trapping of photogenerated charge carriers, adsorption/desorption of reaction components and appropriate redox couples could crucially influence the recombination rate of an electron-hole pair. Even though Ti-C bonds have not been detected on the surface, we suppose that the improvement of photocatalytic activity of nitrogen-containing films is connected with promoting action of carbon in the incorporation of nitrogen atoms into the semiconductor structure (TZ5). It is suggested that the defects in TiO₂/ZrO₂ matrix caused by chemical bonding of N and Ti atoms act as traps for the electron/hole.

4. Conclusions

The influence of synthesis conditions on the efficiency of nitrogen incorporation in the presence of double doping agents (N₂/CH₄) was studied. The presence of low content of CH₄ in deposition ambience (10:1 N₂/CH₄) assisted the formation of O-Ti-N fragments in metal oxide matrix as evidenced from the remarkable appearance of Ti2p_{3/2} ($E_b=457.5$ eV) and N1s ($E_b=395.8$ eV) peaks in XPS spectra. It followed that the nitrogen incorporation induced the traps for charges photogenerated by light leading to the improvement in photocatalytic reduction of toxic Cr(VI) to Cr(III) under UV light.

Acknowledgements

OL, IP, NS, AE, GS, NS, CR and INM acknowledge with thanks the support of this work under the exchange program "Physical and chemical approaches to the synthesis of visible-light sensitive semiconductor films for photo-catalytic application" between Academy of Sciences of Ukraine and Romanian Academy. GS, NS, CR and INM acknowledge with thanks the support of

UEFISCDI under the contract ID 304/2011. VDj and DjJ wish to acknowledge the financial support from Ministry of Science and Technological Development of the Republic of Serbia through the project III 45019.

References

- [1] K. Hashimoto, H. Irie, A. Fujishima, TiO₂ Photocatalysis: A Historical Overview and Future Prospects, *Jpn. J. Appl. Phys.* **44** 8269-8285 (2005)
- [2] M. Anpo, Preparation, Characterization, and Reactivities of Highly Functional Titanium Oxide-Based Photocatalysts Able to Operate under UV-Visible Light Irradiation: Approaches in Realizing High Efficiency in the Use of Visible Light, *Bull. Chem. Soc. Jpn.* **77**, 1427-1442 (2004)
- [3] A. Kudo, H. Kato, I. Tsuji, Strategies for the Development of Visible-light-driven Photocatalysts for Water Splitting, *Chem. Lett.* **33** 1534-1539 (2004)
- [4] T.L. Thompson, J.T. Yates Jr., Surface Science Studies of the Photoactivation of TiO₂ New Photochemical Processes, *Chem. Rev.* **106** 4428-4453 (2006)
- [5] A.K. Ghosh, H.P. Maruska, Photoelectrolysis of Water in Sunlight with Sensitized Semiconductor Electrodes, *J. Electrochem. Soc.* **124** 1516-1522 (1977)
- [6] W. Choi, A. Termin, M.R. Hoffmann, The Role of Metal Ion Dopants in Quantum-Sized TiO₂: Correlation between Photoreactivity and Charge Carrier Recombination Dynamics, *J. Phys. Chem.* **98** 13669-13679 (1994)
- [7] A.L. Linsebigler, G.Q. Lu, J.T. Yates, Photocatalysis on TiO₂ Surfaces: Principles, Mechanisms, and Selected Results, *Chem. Rev.* **95** 735-758 (1995)
- [8] H. Irie, Y. Watanabe, K. Hashimoto, Nitrogen-Concentration Dependence on Photocatalytic Activity of TiO_{2-x}N_x Powders, *J. Phys. Chem. B* **107** 5483-5486 (2003)
- [9] T. Morikawa, R. Asahi, T. Ohwaki, K. Aoki, Y. Taga, Band-Gap Narrowing of Titanium Dioxide by Nitrogen Doping, *Jpn. J. Appl. Phys.* **40** L561-L563 (2001)
- [10] S. Sakthivel, H. Kisch, Photocatalytic and Photoelectrochemical Properties of Nitrogen-Doped Titanium Dioxide, *Chem. Phys. Chem.* **4** 487-490 (2003)
- [11] T. Ohno, M. Akiyoshi, T. Umebayashi, K. Asai, T. Mitsui, M. Matsumura, Preparation of S-doped TiO₂ photocatalysts and their photocatalytic activities under visible light, *Appl. Catal. A-Gen.* **265** 115-121 (2004)
- [12] G. Socol, Yu. Gnatyuk, N. Stefan, N. Smirnova, C. Sutan, V. Malinovski, A. Stanculescu, O. Korduban, I. N. Mihailescu, Photocatalytic activity of pulsed laser deposited TiO₂ thin films in N₂, O₂ and CH₄, *Thin Solid Films* **518** 4648-4653 (2010)
- [13] E. Gyorgy, G. Socol, E. Axente, I. N. Mihailescu, C. Ducu, S. Ciuca, Anatase phase TiO₂ thin films obtained by pulsed laser deposition for gas sensing applications, *Appl. Surf. Sci.* **247** 429-433 (2005)
- [14] D. Caiteanu, E. Gyorgy, S. Grigorescu, I. N. Mihailescu, G. Prodan, V. Ciupina, Growth of oxide thin films for optical gas sensor applications, *Appl. Surf. Sci.* **252** 4582-4586 (2006)
- [15] Ion N. Mihailescu, Carmen Ristoscu, Adriana Bigi, Isaac Mayer, Advanced biomimetic implants based on nanostructured coatings synthesized by pulsed laser technologies, Chapter 10 in "Laser-Surface Interactions for New Materials Production Tailoring Structure and Properties", Series: Springer Series in Materials Science, Vol. 130, Miotello, Antonio; Ossi, Paolo M. (Eds.), pp. 235 – 260 (2010)
- [16] Yu. Gnatyuk, N. Smirnova, A. Eremenko, V. Ilyin, Design and Photocatalytic Activity of Mesoporous TiO₂/ZrO₂ Thin Films, *Adsorption Science & Technology* **23** 497-508 (2005)
- [17] N.V Vituk, N.P. Smirnova, A.M. Eremenko, I.P. Bukov, Influence of high-energy irradiation on formation of defects in individual and mixed oxide SiO₂-TiO₂-ZrO₂, *Surface* **2** ISBN 978-966-00-0834-1, 161-171 (2010)
- [18] D. Briggs, M.P. Seach, Practical surface analysis by Auger and X-ray photoelectron spectroscopy, John Wiley & Sons, Chichester - New York (1983)
- [19] Y. Wang, D.J. Doren, First-principles calculations on TiO₂ doped by N, Nd, and vacancy, *Solid State Commun.* **136** 186-189 (2005)
- [20] M.E. Manriquez, T. Lopez, R. Gomez, J. Navarrete, Preparation of TiO₂-ZrO₂ mixed oxides

- with controlled acid–basic properties, *J. Molec. Catal. A: Chemical*. **220** 229–237 (2004)
- [21] Y. Wan, J. Ma, W. Zhou, Y. Zhu, X. Song, H. Li. Preparation of titania-zirconia composite aerogel materials by sol-gel combined supercritical fluid drying, *Appl. Catal.* **277** 55-59 (2004)
- [22] Y. Nakano, T. Morikawa, T. Ohwaki, Y. Taga, Origin of visible-light sensitivity in N-doped TiO₂ films, *Chem. Phys.* **339** 20-26 (2007)
- [23] C. di Valentin, E. Finazzi, G. Pacchioni, A. Selloni, S. Livraghi, M. C. Paganini, E. Giamello, N-doped TiO₂: Theory and experiment, *Chem. Phys.* **339** 44-56 (2007)
- [24] S.A. Chambers, S.H. Cheung, V. Shutthanandan, S. Thevuthasan, M.K. Bowman, A.G. Joly, Properties of structurally excellent N-doped TiO₂ rutile, *Chem. Phys.* **339** 27-35 (2007)
- [25] Abdul K. Rumaiz, BakhtyarAli, Abdullah Ceylan, M. Boggs, T. Beebe, S. Ismat Shah, Experimental studies on vacancy induced ferromagnetism in undopedTiO₂, *Solid State Communications* **144** 334-338 (2007)
- [26] J.C. Dupin, D. Gonbeau, P. Vinatier, A. Levasseur, Systematic XPS studies of metal oxide, hydroxides and peroxides, *Phys.Chem.Chem.Phys.* **2** 1319-1324 (2000)
- [27] Yu. Gnatuk, N. Smirnova, O. Korduban, A. Eremenko, Effect of zirconium incorporation on the stabilization of TiO₂ mesoporous structure, *Surface and Interface Analysis* **42** 1276-1280 (2010)
- [28] N.C. Saha, H.G. Tompkins, Titanium nitride oxidation chemistry. An X-ray photoelectron spectroscopy study, *J. Appl. Phys.* **72** 3072-3079 (1992)
- [29] J. Yang, H. Bai, Q. Jiang, J. Lian, Visible-light photocatalysis in nitrogen–carbon-doped TiO₂ films obtained by heating TiO₂ gel–film in an ionized N₂ gas, *Thin Solid Films* **516** 1736-1742 (2008)
- [30] J. Yang, H. Bai, X. Tan, J. Lian, IR and XPS investigation of visible-light photocatalysis— Nitrogen–carbon-doped TiO₂ film, *Appl. Surf. Sci.* **253** 1988-1994 (2006)
- [31] S. Somekawa, Y. Kusumoto, M. Ikeda, B. Ahmmad, Yu. Horie, Fabrication of N-doped TiO₂ thin films by laser ablation method: Mechanism of N-doping and evaluation of the thin films, *Catalysis Communications* **9** 437-440 (2008)
- [32] M. Miyauchi, A. Ikezawa, K. Hashimoto, Zeta potential and photocatalytic activity of nitrogen doped TiO₂ thin films, *Phys. Chem. Chem. Phys.* **6** 865-870 (2004)
- [33] L. Mai, C. Huang, D. Wanga, Z. Zhang , Y. Wang, Effect of C doping on the structural and optical properties of sol–gel TiO₂ thin films, *Appl. Surf. Sci.* **255** 9285-9289 (2009)

Measuring Nanolayer Profiles of Various Materials by Evanescent Light Technique

Nina Mirchin¹, Boris Apter¹, Igor Lapsker¹, V. Fogel¹, Uri Gorodetsky¹,
Simona A. Popescu¹, Aaron Peled¹, Gianina Popescu-Pelin², Gabriela Dorcioman²,
Liviu Duta², Andrei Popescu², and Ion N. Mihailescu^{2,*}

¹Photonics Laboratory, EE Department, Holon Institute of Technology, 52 Golomb Str. Holon, Israel- 58102

²National Institute for Lasers, Plasma and Radiation Physics, Lasers Department,
P. O. Box MG-54, RO-77125, Magurele, Ilfov, Romania

The evanescent light photon extraction efficiency of insulator, semiconductor and conductor amorphous nanolayers deposited on glass waveguides was evaluated from Differential Evanescent Light Intensity measurements. The Differential Evanescent Light Intensity technique uses the evanescent field scattered by the deposited nanolayer, enabling nanometer thickness profiling due to the high inherent dark background contrast. The results show that the effective evanescent photon penetration depth increases from metal to semiconductor and then to insulating layers, establishing thus the effective photon-material interaction length for the various materials classes.

Keywords: Evanescent Wave Imaging, Nanofilms, Maxwell Equation Solving, Total Internal Reflection, Thickness Measurement.

1. INTRODUCTION

The morphology profile diagnostic Differential Evanescent Light Intensity (DELI) method^{1,2} is an optical microscopy technique based on capturing the optical field extracted by nanomaterials layers deposited on a waveguide from evanescent fields. The technique uses the phenomenon of Total Internal Reflection (TIR)^{3,4} where evanescent waves occur. This technique has the advantage over reflective or transmission microscopy that the propagating electromagnetic field in the waveguide does not interfere with the photons extracted perpendicular to the substrate surface. An excellent contrast for optical density versus dark background is thus reached enabling nanometer thickness *z*-profiling by optical microscopy.

In this work, DELI profiles for nanostructures of three different classes of materials conductor, semiconductor and insulator i.e., (amorphous Au (a-Au), amorphous Se (a-Se) and polyethylene (PE)) were compared.^{1,2} Basically, by the DELI technique one captures the scattered optical light intensity pattern from deposited particles on a substrate from a light beam propagating through a glass substrate which serves also as light waveguide.

2. NANOMETER FILMS PROFILE EVALUATION BY DELI

In this study a-Au, a-Se and PE nanolayers were chosen as typical metal, semiconductor and insulator amorphous materials respectively and imaged by DELI obtaining characteristic parameters of the evanescent field via a phenomenological model. The visible spectra imaging light beam introduced in the waveguide was supplied by a GE-Thorn, Quartz Halogen lamp, model DDL, with a fiber illuminator, type Volpi AG, having an integrated light intensity of about $I_0 = 3.75 \text{ W/cm}^2$ within the spectral range of 400–800 nm at the fiber tip. The optical image of the evanescent emanating light from the waveguide through its upper face was captured by a microscope Leica Wild M3Z with a magnification of 65–400, equipped with a CCD camera, having a peak wavelength response at 555 nm.

The a-Au films were obtained by sputtering,⁵ a-Se films were obtained by Photodeposition,^{6,7} and the PE nanolayers by Matrix Assisted Pulsed Laser Evaporation (MAPLE).^{8–10}

The DELI technique provides optical density 2D images captured by the CCD camera and then processed by Image Processing techniques to be displayed finally in 3D perspective images as shown for a-Au, a-Se and PE nanolayer samples in Figure 1. In Figure 2 a typical set of DELI

*Author to whom correspondence should be addressed.

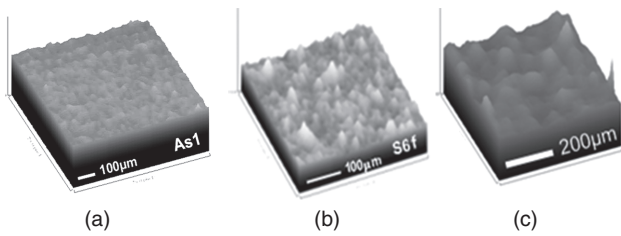


Fig. 1. DELI 3D perspective nano-profile images of sampled areas for (a) a-Au zone, (b) a-Se deposited zone, (c) PE deposited zone.

images of square area samples for a-Au nanolayers and their 1D profile are shown. As visible from Figure 2, for each sample the 2D image of the film has an observable optical density spatial variance $D(x, y)$ which can be interpreted as the normalized intensity $I(x, y)/I_0$ captured by the camera and approximately following the nanometer thickness profile over the deposited area. Beneath the 2D square zones images with areas of $\sim 842 \times 842 \mu\text{m}^2$ the 1D x -direction profiles of the 2D areas averaged over the y -coordinate are shown.

By the DELI method described in detail in Refs. [1, 2], from the 2D nanofilm images captured by the CCD camera, the Normalized Integrated Optical Density (NIOD) is obtained (Eq. (1)) by integration over the whole area and normalized into an effective gray level profile of the imaged zone, i.e.,

$$\text{NIOD} = \frac{\iint_S D(x, y) \cdot ds}{S} \quad (1)$$

In Eq. (1) $D(x, y)$ is the gray level value of each pixel (0-255) and S is the area of the sampled 2D zones. Using a phenomenological model described next, we transformed the NIOD into nanometer layers thickness by calibration.

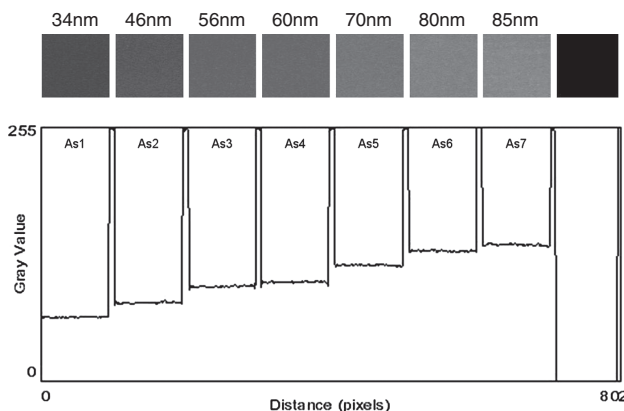


Fig. 2. Upper square figures are the DELI 2D images of the seven a-Au sampled area profiles of $\sim 842 \times 842 \mu\text{m}^2$ for discrete thicknesses in the range (34–85) nm. Beneath the 2D square zones images the 1D profile averaged over vertical y -coordinate across each of the 2D areas are shown. The black zone is for calibration purposes.

3. DELI PHOTON EXTRACTION MODEL

In our DELI technique the light power extracted from the waveguide depends on the thickness and number of deposited nanoparticles on the surface. Due to spatial varying adsorption properties for instance, the nanolayers may have various coverage properties as seen in Figure 1. In the non-deposited areas, complete TIR occurs for the trapped light propagating in the waveguide and no light comes out, see black zone in Figure 2. The nanometer thick deposited areas extract the light from the evanescent waves approximately in proportion to their thickness up to an effective thickness of the photon-material interaction.

Our phenomenological model^{1,2} assumes that the evanescent field in the air close to the waveguide is perturbed by the deposited particles and the extracted evanescent light intensity $I_z(x, y)_{\text{det}}$ arriving at the CCD detector is given by:

$$I_z(x, y)_{\text{det}} = \eta(x, y) \cdot I_0 \quad (2)$$

Here I_0 denotes the optical field intensity at the waveguide/material interface and $\eta(x, y)$ is the photon extraction efficiency function of the deposited material from the propagating field at the waveguide point (x, y) . η has the physical significance of a material-photon extraction efficiency depending on the interaction between the evanescent photons and the deposited particles on the waveguide. In the general case where optical absorption is included,^{1,2} η is given by:

$$\eta(h(x, y)) = (1 - e^{-\gamma h(x, y)}) \cdot e^{-\alpha h(x, y)} \quad (3)$$

We considered the ability of the nano-deposited material to extract the evanescent photons from the waveguide to be characterized by a constant γ , and the absorption of light in the nanolayer by the optical absorption constant, α . $h(x, y)$ is the deposited material thickness in the z -direction at point (x, y) on the waveguide surface.

Typically for thicknesses less than 200 nm (the exact value depending on the material type) one may neglect the optical absorption in the thin films and use the simpler Eq. (4).

$$\eta(h(x, y)) \approx (1 - e^{-\gamma h(x, y)}) \quad (4)$$

In the literature,⁴ a parameter denoted by d is defined as the penetration depth of the evanescent field from the waveguide into a low refractive index media, expressing the decaying length of the evanescent field at the interface. It is related to the refractive index of the two media n_1, n_2 , free space wavelength λ_{vac} of the light beam used and the incidence angle θ_i by:

$$d = \frac{\lambda_{\text{vac}}}{2 \cdot \pi \cdot \sqrt{n_1^2 \cdot \sin^2 \theta_i - n_2^2}} \quad (5)$$

n_1 is the waveguide refractive index and n_2 is the refractive index of the second media above the waveguide.

Using γ from Eq. (4) the penetration depth of the evanescent field photons into the deposited material can be estimated by $d \approx \gamma^{-1}$ assuming thus that it is the effective range into the material, responsible for proportionally extracting evanescent field photons from the waveguide.

4. DELI APPLICATION

When the optical absorption can be neglected, which is valid for most nanometer thick layers, the following NIOD ratio for two nanolayer of h_1 and h_2 thickness is obtained from Eq. (4):

$$\frac{\text{NIOD}_2(h_2)}{\text{NIOD}_1(h_1)} \approx \frac{\eta_2}{\eta_1} = \frac{(1 - e^{-\gamma h_2})}{(1 - e^{-\gamma h_1})} \tag{6}$$

where $h_1(x, y)$ and $h_2(x, y)$ are the thickness corresponding to two different locations on film. Measuring for two points the NIOD ratio gives thus the value of γ and relative thickness profiles for other locations or samples.

For absolute thickness calibration, h_1 or h_2 can be measured by independent techniques such as Spectrometric, SEM, AFM or nanoprofilometry, and absolute surface thickness $h(x, y)$ profiles can be mapped using the NIOD values and γ .⁵⁻⁷ A typical plot of the thicknesses as obtained from Eq. (6) for a-Au samples as a function of deposition time is given in Figure 3, demonstrating the usefulness of the DELI technique in evaluating nanometer thickness in nanolayer materials deposition processes. In this particular case the absolute calibration was conducted by nanoprofilometry.

The evanescent photon “extraction ability” included in the constant γ can be further determined experimentally as follows. We define a parameter K as:

$$K = \eta_2/\eta_1 \tag{7}$$

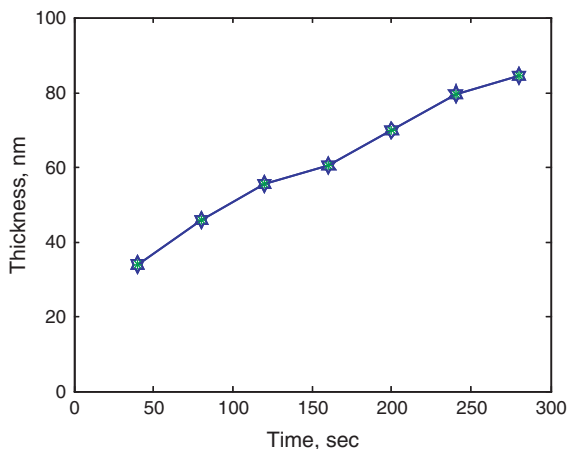


Fig. 3. Plot of the DELI evaluated thickness obtained from Eq. (6) for a-Au samples deposited by sputtering as a function of deposition time.

Table I. Photon extraction parameter γ and evanescent penetration depth d for different materials types and thicknesses.

Material	a-Au	a-Se	PE
η_1	38.90	30	32.7
h_1 , nm	26.3	40	83
η_2	73.47	80	68.3
K	1.9	2.7	2.1
γ , nm ⁻¹	0.0284	0.0116	0.00779
d , nm	35.2	86.5	128.3

for two points with thicknesses $h_2 > h_1$. For $K > 1$ by using Eq. (6) with a tolerance set at $(e^{-\gamma(h_2-h_1)}/K) \ll 1$ we obtain:

$$K/(K - 1) \approx e^{\gamma h_1}. \tag{8}$$

Hence

$$\gamma \approx h_1^{-1} \ln(K(K - 1)^{-1}). \tag{9}$$

From the DELI measurements of the materials in this study we obtained for the evanescent photon extraction parameter γ and the “effective evanescent photon penetration depth,” d , the values given in Table I.

As seen from Table I the penetration depth d of the evanescent photons into the material covering the waveguide for a-Au is smaller than for the semiconductor a-Se and insulating material PE. This means that the metallic has a shortest evanescent extraction range in respect with semiconductor and insulator material. It results that for evaluating nanolayer thicknesses ranges for various materials classes by DELI one can be guided by the characteristic value of the parameter $d \approx \gamma^{-1}$.

5. CONCLUSIONS

We used the results of the nanometer profile diagnostic method DELI,^{1,2,5-7} to compare the photon extraction efficiency of different materials i.e., conductor a-Au, semiconductor a-Se and insulator PE nanolayers deposited on glass waveguides. The DELI technique, based on capturing the evanescent field scattered by a nanolayer has the advantage over reflective or transmission microscopy that the propagating electromagnetic field in the waveguide does not interfere with the field extracted perpendicular to the substrate surface. It thus guaranties an excellent dark background contrast enabling direct depth z -direction optical microscopy nanometer thickness profiling. For insulator nanolayers the technique has a longer range of interaction with the evanescent photons as compared to semiconductors and conductors. Accordingly, thicker films fall in the range suitable for DELI nanometer profiling, up to about 200 nm. There is no risk of nanomaterials damage because they are not exposed in DELI to the direct action of intense light or electron beams. The technique is much easier and economical for nanometer films profiling

as compared to SEM and AFM and suited especially for large areas profiling needed in industrial applications.

Acknowledgments: Gianina Popescu-Pelin, Gabriela Dorcioman, Liviu Duta, Andrei Popescu and Ion N. Mihailescu acknowledge the financial support of this work under the contract ID 304/2011.

References and Notes

1. G. Socol, E. Axente, M. Oane, L. Voicu, A. Petris, V. Vlad, I. N. Mihailescu, N. Mirchin, R. Margolin, D. Naot, and A. Peled, *Appl. Surf. Sci.* 253, 6535 (2007).
2. G. Socol, E. Axente, M. Oane, L. Voicu, A. Dinescu, A. Petris, V. Vlad, I. N. Mihailescu, N. Mirchin, R. Margolin, D. Naot, and A. Peled, *J. Mater. Sci.-Mater. Electron.* 18, 207 (2007).
3. L. Novotny and B. Hecht, *Principles of Nano-optics*, Cambridge University Press, New York (2006).
4. F. de Fornel, *Evanescent Waves: From Newtonian Optics To Atomic Optics*, Springer-Verlag Berlin and Heidelberg, New York (2001).
5. V. Fogel, N. Mirchin, S. Popescu, I. Lapsker, and A. Peled, *J. Optoelectron. Adv. Mater.* 10, 2482 (2008).
6. S. A. Popescu, B. Apter, N. Mirchin, I. Lapsker, and A. Peled, *Journal of Advanced Research in Physics* 1, 011010 (2010).
7. S. Aaronov, E. Ganon, P. Okhman, M. Gankin, N. Mirchin, S. A. Popescu, I. Lapsker, and A. Peled, *J. Nanophotonics* 3, 031785 (2009).
8. R. Cristescu, E. Axente, G. Socol, A. Moldovan, D. Mihaiescu, I. Stamatina, T. Buruiana, M. Jelinek, I. N. Mihailescu, and D. B. Chrisey, *Laser Phys.* 15, 1686 (2005).
9. R. Cristescu, G. Dorcioman, C. Ristoscu, E. Axente, S. Grigorescu, A. Moldovan, I. N. Mihailescu, T. Kocourek, M. Jelinek, M. Albulescu, T. Buruiana, D. Mihaiescu, I. Stamatina, and D. B. Chrisey, *Appl. Surf. Sci.* 252, 4647 (2006).
10. M. Jelinek, T. Kocourek, J. Remsa, R. Cristescu, I. N. Mihailescu, and D. B. Chrisey, *Laser Phys.* 17, 66 (2007).

Received: 18 August 2011. Accepted: 9 November 2011.

Delivered by Ingenta to:
Hebrew University of Jerusalem
IP : 128.139.19.24
Mon, 09 Jul 2012 07:26:08

